

# Trapped particles and asymmetry-induced transport<sup>a)</sup>

A. A. Kabantsev,<sup>b)</sup> J. H. Yu, R. B. Lynch, and C. F. Driscoll

*Physics Department and Institute for Pure and Applied Physical Sciences, University of California at San Diego, La Jolla, California 92093*

(Received 11 November 2002; accepted 4 February 2003)

Trapped particle modes and the associated asymmetry-induced transport are characterized experimentally in cylindrical electron plasmas. Axial variations in the electric or magnetic confinement fields cause the particle trapping, and enable the  $\mathbf{E} \times \mathbf{B}$  drift trapped-particle modes. Collisional diffusion across the trapping separatrix causes the modes to damp, and causes bulk radial transport when the confinement fields also have  $\theta$  asymmetries. The measured asymmetry-induced transport rates are directly proportional to the measured mode damping rates, with simple scalings for all other plasma parameters. Significant transport is observed for even weak trapping fields ( $\delta B/B \sim 10^{-3}$ ), possibly explaining the “anomalous” background transport observed so ubiquitously in single species plasmas. © 2003 American Institute of Physics.

[DOI: 10.1063/1.1564089]

## I. INTRODUCTION

Containment of single species plasmas in cylindrical Penning–Malmberg traps is used for a variety of experiments and applications in fundamental plasma physics, two-dimensional (2D) ideal fluid dynamics, Coulomb crystals, precision spectroscopy, frequency standards, and antimatter confinement.<sup>1</sup> These plasmas have exceptional confinement properties compared to neutral or quasineutral plasmas, since radial expansion is constrained by the conservation of canonical angular momentum  $P_\theta$ .<sup>2</sup> There are also constraints placed on the expansion by conservation of total energy and by adiabatic invariants associated with the kinetic energy of the particles. However, small  $\theta$  asymmetries in the trapping fields can exert negative torques which change the total angular momentum and cause slow radial expansion of the plasma. The broad scaling characteristics of this “anomalous” background transport have been measured experimentally over the past 20 years,<sup>3–9</sup> but theoretical understanding of the transport kinetics has developed only in a few limited parameter regimes.<sup>10</sup>

Here we present measurements which unambiguously demonstrate that the dominant asymmetry-induced transport mechanism on the “CamV” apparatus involves diffusion across the velocity-space separatrix between axially trapped and passing particles; and that these dissipative separatrix crossings also cause damping of the observed trapped-particle modes. Similar trapped-particle  $\mathbf{E} \times \mathbf{B}$  drift modes and instabilities have been extensively analyzed theoretically<sup>11–13</sup> for neutral plasmas; and instability has been identified experimentally in some regimes.<sup>14</sup> In cylindrical traps, axial trapping occurs naturally due to  $\theta$ -symmetric variations in the magnetic field strength with  $\delta B/B \sim 10^{-3}$ ; and we also apply larger controlled magnetic and electric trapping fields.

With controlled electric trapping, trapped-particle modes with various  $m_\theta$  and  $k_z$  are readily observed<sup>15</sup> at frequencies below the plasma  $\mathbf{E} \times \mathbf{B}$  rotation frequency, i.e.,  $f \lesssim m_\theta f_E$ . The mode consists of trapped particles on either side of an electrostatic potential barrier which execute  $\mathbf{E} \times \mathbf{B}$  drift oscillations that are 180° out of phase, while passing particles move along field lines to Debye shield the potential from trapped particles. The main damping of this mode is due to separatrix diffusion, and an analytic treatment is being developed.<sup>16</sup> These dissipative separatrix crossings can also be induced by resonant rf fields, allowing the process to be investigated in detail.<sup>17</sup>

When static  $k_z \neq 0$ ,  $m_\theta \neq 0$  asymmetries (such as a magnetic “tilt”) exist in the trapping fields, the plasma equilibrium necessarily has dc “asymmetry currents” driven by the  $\mathbf{E} \times \mathbf{B}$  drift rotation through the static asymmetries. Similar tilt-induced *slushing* currents at the diocotron mode frequency have been previously identified,<sup>18</sup> but not analyzed in depth. When some particles are axially trapped, the field asymmetry creates different drift orbits for trapped and passing particles. The transport then results from neoclassical steps taken by particles when scattered across the separatrix. Equivalently, one may say that collisional diffusion across the trapping separatrix dissipates these currents and causes bulk radial transport in the same way as it damps the trapped particle modes. Indeed, one can describe the dc currents as driving the trapped particle mode off resonance.

Experiments over a wide range of parameters show that the tilt-asymmetry-induced transport rate is directly proportional to the trapped particle mode damping rate  $\gamma_a$ , when applied electric barriers create a significant trapped particle population. When  $\gamma_a$  is factored out, the transport rates are observed to follow simple scalings with plasma parameters such as magnetic field  $B$ , line density  $N_L$ , length  $L_p$ , and tilt angle  $\alpha_B$ .

Magnetic trapping barriers appear to give generically similar transport, and are probably the cause of anomalous background transport in many long cylindrical traps.

<sup>a)</sup>Paper Q12 3, Bull. Am. Phys. Soc. **47**, 250 (2002).

<sup>b)</sup>Invited speaker. Electronic mail: aakpla@physics.ucsd.edu

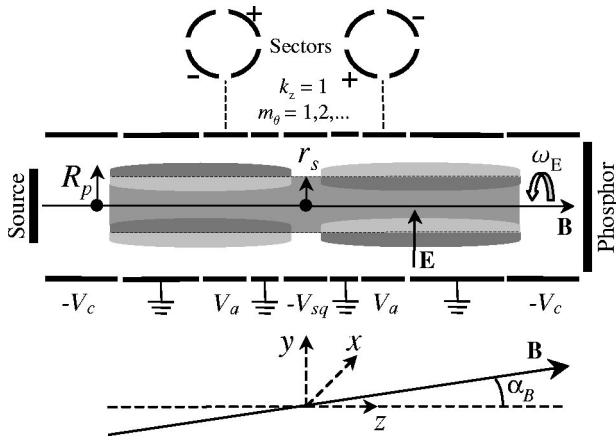


FIG. 1. Schematic of electron plasma with a trapped particle mode in the cylindrical containment system.

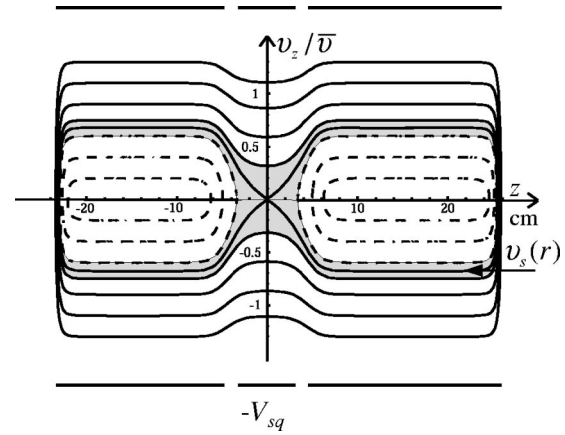


FIG. 2. Phase-space orbits with an applied squeeze potential. The effect of collisions is greatly enhanced in the shaded separatrix region.

Asymmetry-induced transport is readily observed both from controlled magnetic barriers and from very small construction ripples in the field strength. The associated modes have not yet been identified experimentally, possibly because they are very strongly damped, and the theory is less well developed. Nevertheless, experimental techniques such as resonant enhancement of separatrix diffusion and combinations of electric and magnetic barriers allow the separatrix-crossing effects to be investigated in detail. Surprisingly, the transport due to magnetic trapping can remain dominant even for exceedingly small  $\delta B/B$ , making it likely that these effects are endemic to long traps.

The experiments presented here focus on  $m_\theta=1, k_z=1$  (tilt) asymmetries. However, trapped particle modes are readily observed for higher  $m_\theta$ , and multiple trapping barriers give rise to higher  $k_z$ . Asymmetries with any  $(m_\theta, k_z)$  will generate equilibrium currents; and strong transport will result if trapping barriers have created geometrically similar separatrices. This mechanism may thus have wide applicability for asymmetry-induced transport.

## II. EXPERIMENTAL SETUP

The experiments are performed on a magnetized pure electron plasma confined in the cylindrical ‘‘CamV’’ apparatus,<sup>19,20</sup> as shown in Fig. 1. A hot tungsten source injects electrons which are contained axially by voltages  $-V_c = -100$  V applied to end cylinders. A strong axial magnetic field ( $0.3 \text{ kG} \leq B \leq 10 \text{ kG}$ ) provides radial confinement. The magnetic field can be aligned with the cylindrical electrode axis, or tilted at an angle  $0 \leq \alpha_B \leq 3 \times 10^{-3}$  rad, giving an  $m_\theta=1, k_z=1$  magnetic asymmetry. A negative ‘‘squeeze’’ voltage  $-V_{sq}$  applied to a central cylinder generates a trapping barrier, with velocity-space separatrix shown schematically in Fig. 2.

The  $z$ -averaged electron density  $n(r, \theta, t)$  can be destructively measured at any time by axially dumping the electrons onto a phosphor screen imaged by axially dumped electrons onto a phosphor screen imaged by a charge-coupled device (CCD) camera. The plasma typically has a central density  $n_o \approx 1.5 \times 10^7 \text{ cm}^{-3}$ , with a length varied over the range  $38 \leq L_p \leq 49$  cm, bounded by a wall radius  $R_w = 3.5$  cm. The electron space charge creates a central potential  $-\phi_p$

$\approx (-30 \text{ V})(N_L/6 \times 10^7)$ , and the radial electric field causes  $\mathbf{E} \times \mathbf{B}$  rotation at a rate  $f_E(r) \equiv cE(r)/2\pi rB \approx (100 \text{ kHz}) \times (n/10^7)(B/1 \text{ kG})^{-1}$ . Figure 3 shows typical profiles of density and rotation.

We adjust the plasma radius over the range  $0.9 \leq R_p \leq 1.5$  cm, which varies the line density  $N_L \equiv \int d\theta r dr n(r, \theta, t)$  over the range  $3 \leq N_L \leq 10 \times 10^7 \text{ cm}^{-1}$ . The electrons have a controllable thermal energy  $0.5 \leq T \leq 6$  eV, giving an axial bounce frequency  $f_b \equiv \bar{v}/2L_p \approx (0.5 \text{ MHz})T^{1/2}(L_p/49)^{-1}$  and a Debye shielding length  $\lambda_D \approx (0.25 \text{ cm})T^{1/2}(n/10^7)^{-1/2}$ . Thus, the plasma ‘‘rigidity’’  $\mathcal{R} \equiv f_b/f_E$  varies over the range  $1 \leq \mathcal{R} \leq 100$ .

Sector wall cylinders are used to excite and detect waves in the plasma. These sector cylinders can also be used to apply a static electric tilt to the plasma with  $k_z \approx 1$ , and  $m_\theta=1$  or 2. A single wall sector can be used as a receiver, or sectors can be used in combination to verify the  $\theta$  and  $z$  symmetries of modes.

Locally trapped particles occur due to unavoidable variations  $\delta B(z)$  in the magnetic field strength, and due to axial variations in the wall voltages. Electric trapping from the externally controlled  $V_{sq}$  causes electrons with axial velocity less than the separatrix velocity  $v_s(r)$  to be trapped axially in one end or the other. For small  $V_{sq}$ , a fraction

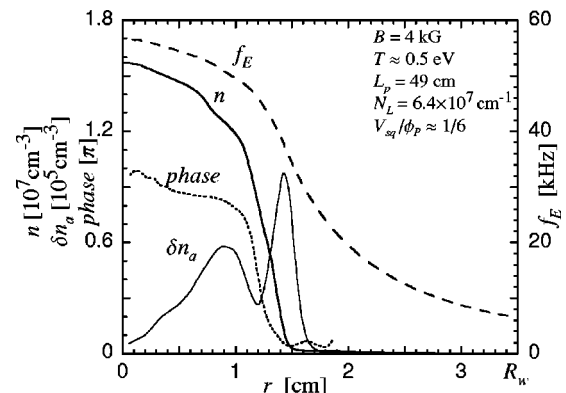


FIG. 3. Measured plasma density  $n(r)$  and resulting  $\mathbf{E} \times \mathbf{B}$  rotation  $f_E(r)$ . Also shown is the radial eigenfunction  $\delta n_a(r)$  for the trapped particle mode.

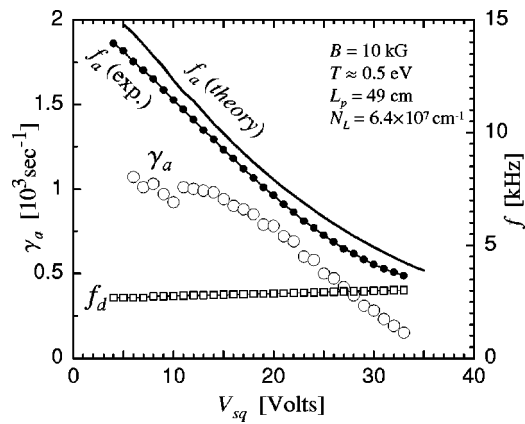


FIG. 4. Mode frequencies  $f_a$  and  $f_d$  and decay rate  $\gamma_a$  vs squeeze voltage  $V_{sq}$  from experiments and theory.

$$\frac{N_L^{\text{tr}}}{N_L} \approx 1.2 \left( \frac{V_{sq}}{\phi_p} \right) \quad (1)$$

of all the electrons are trapped. The potential barrier from  $V_{sq}$  increases in strength with  $r$ , so most of the trapped particles are near the radial edge of the plasma at  $r \geq r_s$ , where  $r_s$  is defined by  $v_s(r_s) = \bar{v}$ .

Figure 2 shows the expected phase space orbits along a sample magnetic field line (e.g., at  $r \sim r_s$ ) for an electrically squeezed equilibrium. The dashed/solid lines represent trapped/passing particle orbits. The shadowed region represents the boundary layer near the separatrix where most of the diffusion occurs.

Magnetic trapping is produced from a  $z$ -localized increase  $\delta B$  in the magnetic field  $B$ , giving a mirror ratio  $\beta \equiv \delta B/B$ . Here the separatrix makes an angle  $\tan^{-1}(\beta^{1/2})$  with  $v_{\perp}$ , and is roughly independent of radius. Inherent magnetic trapping always exists in our apparatus due to small ( $\beta \sim 10^{-3}$ ) magnetic ripples in the superconducting magnet. Larger values of  $\delta B$  are obtained from a squeeze magnet, which is a  $z$ -localized warm magnetic coil, giving  $\beta < 0.04$  over a region  $\Delta z \lesssim 10$  cm.

### III. TRAPPED-PARTICLE MODE WITH ELECTRIC TRAPPING

Experimentally, the  $m_{\theta} = 1$  “trapped-particle diocotron mode” is excited on an electrically squeezed plasma with a short burst of 1–10 sinusoidal oscillations that are phased + and – on  $\theta$ -opposed and  $z$ -opposed wall sectors, as shown in Fig. 1. Using other wall sectors as antennae, the mode waveform is digitized as the mode “rings down,” giving accurate measurements of frequency and damping rate.

Figure 4 shows the measured trapped-particle mode frequencies  $f_a$  and damping rates  $\gamma_a$  as the applied squeeze voltage  $V_{sq}$  is varied. The venerable  $m_{\theta} = 1$ ,  $k_z = 0$  diocotron mode frequency  $f_d$  is also shown. As  $V_{sq}$  increases,  $f_a$  decreases from near the edge plasma rotation frequency  $f_E(R_p)$  at low  $V_{sq}$  to the diocotron mode frequency  $f_d$  at  $V_{sq} \geq \phi_p$ . At large  $V_{sq}$ , the plasma is essentially cut in half, and on either side of the barrier the plasma supports  $k_z = 0$  (diocotron) drift orbits which are  $180^\circ$  out of phase. Even for

small  $V_{sq}$ , the trapped particle mode is essentially uniform with  $z$  on either side of the barrier, changing sign at the barrier. A simple kinetic theory model with a zero-length trapping barrier<sup>15</sup> predicts mode frequencies agreeing with measurements to within 10%, as shown in Fig. 4.

The eigenfunction  $\delta n_a(r)$  for the mode is obtained from separate camera measurements of the density  $n_h(r, \theta, t)$   $z$ -averaged over half the plasma. That is,  $V_{sq}$  is raised to  $-100$  V immediately before lowering  $V_c$  to dump the electrons onto the phosphor. The time sequence of density data is fit to an  $m_{\theta} = 1$  perturbation as

$$n_h(r, \theta, t) = \int d\theta \widetilde{\delta n}_a(r) \exp\{-im_{\theta}\theta + i2\pi f_a t - \gamma_a t\}. \quad (2)$$

Figure 3 shows the magnitude  $\delta n_a(r)$  and phase of the complex eigenfunction  $\widetilde{\delta n}_a(r)$ . The outer peak at  $r > 1.2$  cm is predominantly trapped particles executing  $\mathbf{E} \times \mathbf{B}$  drift orbits. The inner peak at  $r < 1.2$  cm is predominantly passing particles, which partially Debye shield the trapped particle perturbation. The minimum of  $\delta n(r)$  is observed at  $r \approx r_s$ , and moves radially inward as  $V_{sq}$  is increased. We note that the phase change between peaks (here  $\approx 0.8\pi$ ) consistently differs from  $\pi$  by more than experimental uncertainty, presumably due to damping effects. This subtlety was missed in prior experiments.<sup>15</sup>

The trapped particle mode is observed to be strongly damped, with  $\gamma_a \approx 1 \times 10^3 \text{ s}^{-1}$  (i.e.,  $\gamma_a/f_a \sim 1/15$ ) for small  $V_{sq}$  at  $B = 10$  kG. Figure 4 shows that the damping rate decreases as  $V_{sq}$  increases, with  $\gamma_a \rightarrow 0$  when the column is cut in half.

Theory work in progress<sup>16</sup> provides some insight into the damping process. The trapped-particle mode dynamics consists of trapped particles moving radially as they  $\mathbf{E} \times \mathbf{B}$  drift in the perturbed azimuthal electric field, while passing particles move axially in an attempt to shield the trapped-particle density perturbation. Thus, particles on either side of the separatrix are involved in completely different types of motion and there is a discontinuity in the perturbed particle distribution function. As a result, electron–electron collisions produce a flux of particles across the separatrix. This continual trapping and detraping of particles results in radial transport of particles and mode damping, and is readily observed in computer simulations.<sup>21</sup>

These collisions at rate  $\nu$  can be treated by a Fokker–Planck collision operator, in an analysis similar to that used for the dissipative trapped-ion instability by Rosenbluth, Ross, and Kostomarov.<sup>13</sup> The collision operator contains velocity derivatives that become arbitrarily large near the discontinuity, so the mode behavior is affected even when collisions are weak. The analysis suggests that velocity space diffusion acting for one mode period will smooth out the discontinuity over a width  $\delta v_{\parallel} \approx \bar{v} \sqrt{\nu/f_E}$ , and that the damping will include this dependence. The square root provides a significant enhancement, since  $\nu/f_E$  is small. One expects the damping rate to have a strong and complicated temperature dependence through the density of particles at the separatrix velocity  $v_s(r)$ , through the collisional frequency  $\nu$ ,

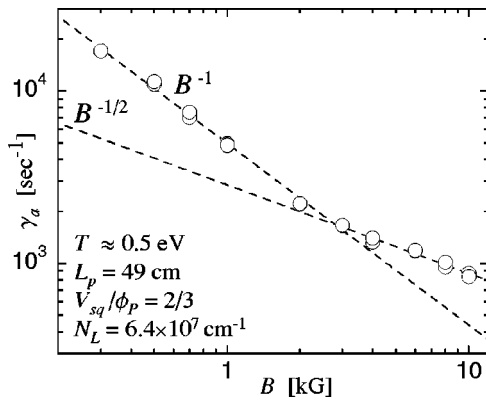


FIG. 5. Mode damping rate vs magnetic field. At high fields where the theory is valid, the predicted  $B^{-1/2}$  scaling agrees with experiments.

and through the Debye shielding length  $\lambda_D$ ; and to possibly include fractional powers of  $B$  as in  $\delta v_t$ .

Figures 5 and 6 show the measured dependencies of  $\gamma_a$  on  $B$  and  $T$ . The measured damping scales approximately as  $\gamma_a \propto B^{-1}$  for  $B \leq 3$  kG (where  $\mathcal{R} \leq 5$ ), and as  $\gamma_a \propto B^{-1/2}$  for high fields. This dependence was missed in early experiments<sup>15</sup> because it was counterbalanced by concurrent transport-induced temperature changes.

Figure 6 shows that  $\gamma_a$  decreases strongly with temperature above  $T \sim 1$  eV. The dashed lines are merely guides for the eye, with the generic functional form  $a[1 - \exp(-b/T)]$ . Preliminary theory results<sup>16</sup> agree qualitatively with these measurements, but substantial questions remain.

It is instructive to consider the balance of energy during the trapped-particle mode decay. As collisions scatter particles across the separatrix, the net result is that trapped particles are transported from the side of low potential perturbation to the high side. In the process, the wave does work on these particles, and electrostatic energy is converted into thermal energy. Since the trapped-particle mode is actually a negative energy wave (like the normal diocotron mode), this process alone would increase the amplitude of the wave. However, passing particles that become trapped after suffering a collision must take a radial step, since their bounce-averaged azimuthal electric field is no longer zero. On average, more newly trapped particles move outward than

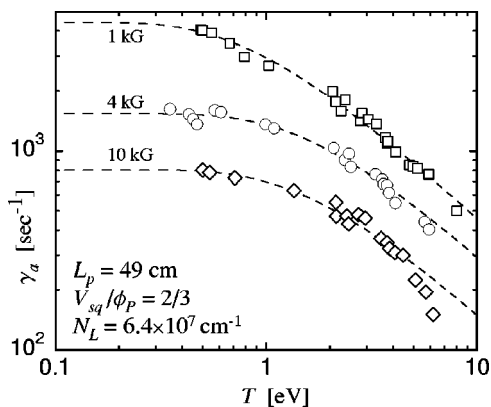


FIG. 6. Mode damping rate vs temperature. The dashed lines are merely guides for the eye, with the generic functional form  $a[1 - \exp(-b/T)]$ .

inward. Electrostatic energy is transferred into the wave as particles move radially outward against the equilibrium electric field, and this process damps the negative energy wave. It turns out the the latter effect of radial transport overwhelms the heating effect and the wave is damped.

#### IV. TRANSPORT WITH ELECTRIC TRAPPING

When  $\theta$ -asymmetries exist in the electric or magnetic confinement fields, they create torques which change the canonical angular momentum of the plasma, causing the average radius to vary. If the asymmetry is nonstatic, the sign of the torque can be positive or negative. The “rotating wall” confinement technique utilizes wall voltages rotating faster than  $f_E$  to obtain plasma compression.<sup>22,23</sup> For the experiments performed here, the  $\theta$ -asymmetries are static in the lab frame and exert a negative torque on the electrons, resulting in bulk radial expansion of the plasma.

Here, we focus on the  $m_\theta = 1, k_z = 1$  magnetic asymmetry induced by a magnetic tilt, with  $\mathbf{B} = B(\hat{z} + \alpha_B \hat{y})$ .

The plasma angular momentum is given by

$$P_\theta \approx \left[ -\frac{eB}{c}(R_w^2 - \langle r^2 \rangle) + m \langle r v_\theta \rangle \right] N_{\text{tot}}, \quad (3)$$

where the  $\langle \rangle$  represents an average over all particles. For strongly magnetized electron columns, the kinetic momentum  $mrv_\theta$  is negligible. The angular momentum is then proportional to  $\langle r^2 \rangle$ , and  $\theta$ -asymmetries cause bulk plasma expansion. The overall asymmetry-induced transport rate is defined by the rate of plasma expansion

$$\nu_p \equiv \frac{1}{\langle r^2 \rangle} \frac{d\langle r^2 \rangle}{dt} \approx \frac{1}{P_\theta} \frac{dP_\theta}{dt}. \quad (4)$$

Transport measurements are typically made by taking two measurements of  $n(r, \theta, t)$  separated in time by  $\Delta t = 0.1 - 20$  s, chosen so that the plasma expansion  $\delta\langle r^2 \rangle / \langle r^2 \rangle \approx 0.02$ . By keeping the plasma expansion roughly constant, the undesirable effect of temperature increase (due to expansion) during  $\Delta t$  is minimized.

We have found that the transport rate  $\nu_p$  is directly proportional to the damping rate  $\gamma_a$  which is observed when the trapped particle mode is excited. This is shown in Fig. 7 for a wide range of plasma parameters  $B, N_L, L_p, V_{sq}$ , for magnetic tilt  $\alpha$  and for one 3 mrad electric “tilt” (E3,  $\nu_p/5$  plotted). This provides strong experimental support for the idea that a common physical mechanism is responsible for both particle transport and trapped-particle mode damping, namely velocity-space diffusion across the separatrix. The measured asymmetry-induced transport rates  $\nu_p$  have rather complicated dependencies on plasma parameters; but  $\nu_p$  has a simple proportionality to  $\gamma_a$ .

In Fig. 8, we plot the normalized transport rate  $\nu_p/\gamma_a$  versus magnetic field  $B$  with other plasma parameters and the applied asymmetry held constant. The normalized expansion rate shows a robust  $B^{-1}$  scaling over more than a decade change in magnetic field. Each point here is a slope obtained from tens of individual points  $\nu_p(\gamma_a)$  by varying only  $T$  and  $\gamma_a(T)$  through standard rf wiggle heating of the plasma.<sup>24,25</sup>

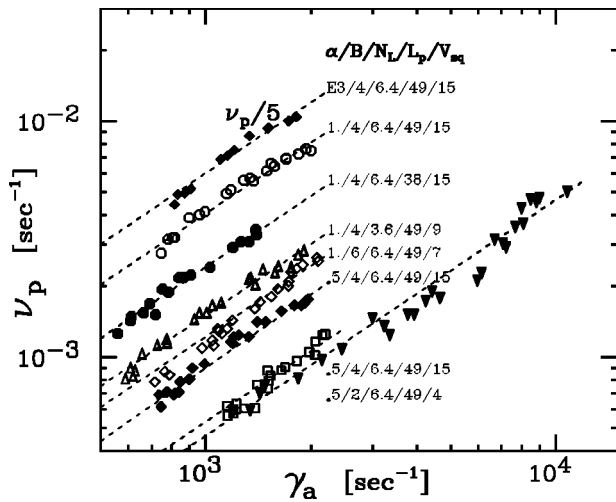


FIG. 7. Measured tilt-induced transport rate  $\nu_p$  vs the simultaneously measured mode damping rate  $\gamma_a$  for a variety of plasma, asymmetry, and trapping parameters.

The scaling of  $\nu_p/\gamma_a$  with line density  $N_L$  depends on whether an electric or magnetic asymmetry is applied. Figure 9 shows  $\nu_p/\gamma_a$  versus  $N_L$  for both types of asymmetries. For a magnetic tilt, we obtain  $\nu_p/\gamma_a \propto N_L^2$ . For an applied electric “tilt” (discussed below), we obtain  $\nu_p/\gamma_a \propto N_L^0$ . Here, we are keeping the fraction of trapped particles  $N_L^{tr}/N_L \propto V_{sq}/\phi_p$  constant. These scalings were observed in early experiments<sup>5-7,26</sup> without a clear understanding of the underlying transport mechanism.

Data sets taken with controlled individual variations in  $B$ ,  $n$ ,  $R_p$ ,  $L_p$ ,  $T$ ,  $V_{sq}$ , and  $\alpha_B$  have now established that in the presence of a magnetic tilt asymmetry, the overall transport scaling is

$$\frac{\nu_p}{\gamma_a} \approx 7.5 \times 10^{-5} \left( \frac{V_{sq}}{\phi_p} \right) \left( \frac{eN_L^2}{B} \right) \left( \frac{L_p}{R_w} \right)^2 \alpha_B^2. \quad (5)$$

Figure 10 shows all measured values of  $\nu_p/\gamma_a$ , with each point being a slope of a data set as in Fig. 7. We find that the magnetic-tilt-induced transport in plasmas with a significant

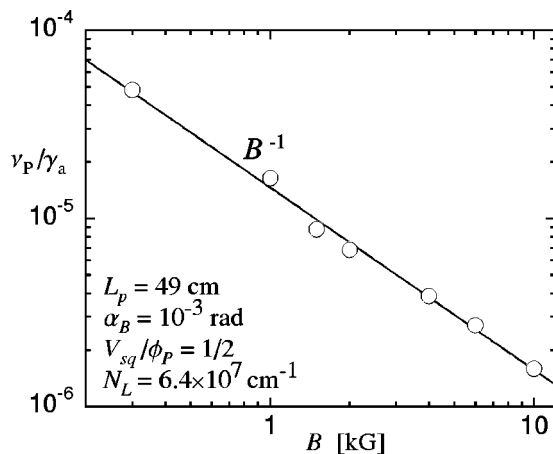


FIG. 8. Normalized transport rate  $\nu_p/\gamma_a$  at constant plasma parameters and applied asymmetry vs magnetic field.

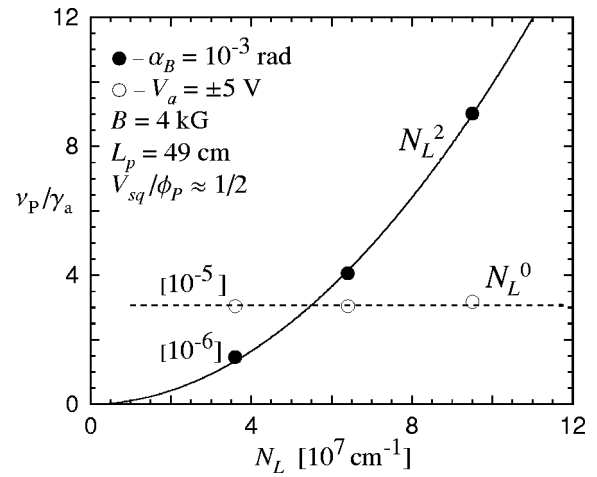


FIG. 9. Normalized transport rate  $\nu_p/\gamma_a$  at constant fraction of trapped particles ( $V_{sq}/\phi_p$ ) vs plasma line density  $N_L$  for magnetic and electric asymmetries.

fraction of electrically trapped particles is proportional to the trapped particle mode damping rate, over a parameter range of 3 decades in  $\nu_p/\gamma_a$ .

Similarly simple transport scalings are obtained for applied  $m_\theta = 1$  electrostatic asymmetries, alone or in combination with a magnetic tilt asymmetry. Figure 11(a) shows the unnormalized transport rate  $\nu_p$  versus static asymmetry voltages  $V_{ax}$  or  $V_{ay}$  applied as  $\pm$  pairs to opposing wall sectors oriented in the  $\hat{x}$  or  $\hat{y}$  directions, in combination with an  $\alpha_{By}$  magnetic tilt. Figure 11(b) shows similar curves obtained for  $\nu_p$  versus magnetic tilts  $\alpha_{Bx}$  or  $\alpha_{By}$  in the  $\hat{x}$  or  $\hat{y}$  directions, in the presence of a  $\hat{y}$  electric tilt. For both electric and magnetic tilts, the transport rates scale quadratically with asymmetries near the minimum in  $\nu_p$ . The deviation from this quadratic scaling at larger  $\nu_p$  (dashed line) is due to an increase of the plasma temperature caused by fast radial expansion. Figure 11 also demonstrates that an electric tilt can partially cancel a magnetic tilt, and vice versa, placing both types of asymmetries on equal footing in terms of transport.

Indeed, we define an electric tilt angle  $\alpha_E$  based on the radial (off-axis) shift  $\Delta$  that an electric asymmetry induces

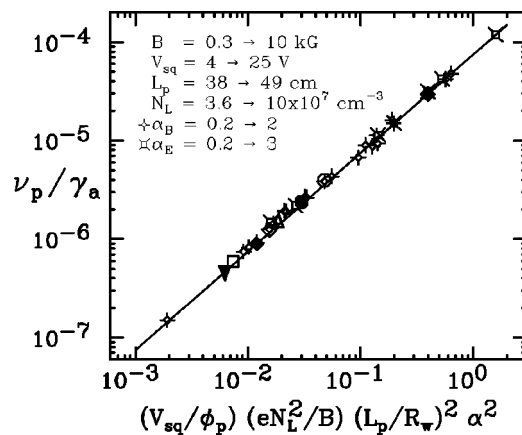


FIG. 10. Measured normalized transport rate  $\nu_p/\gamma_a$  vs scalings for all plasma parameters.

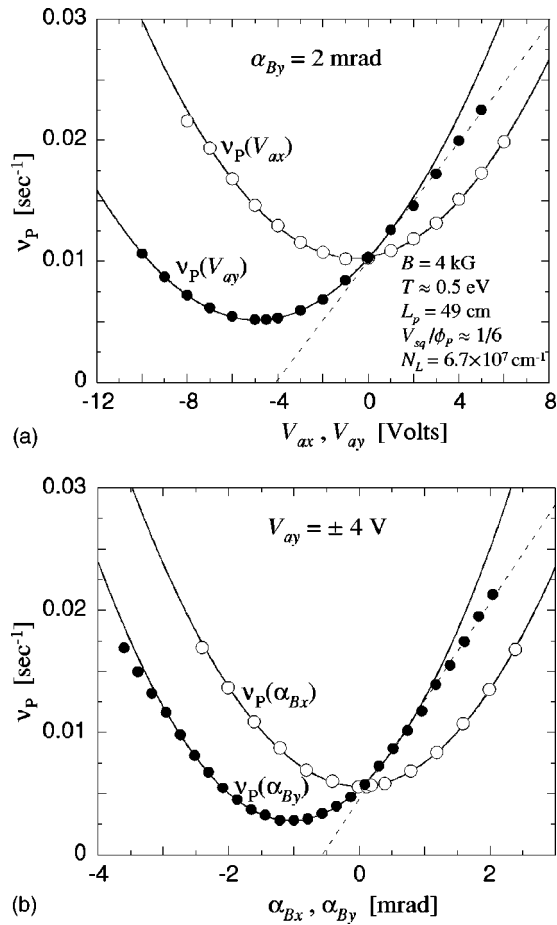


FIG. 11. Measured transport rate  $\nu_p$  from a static asymmetry voltage with simultaneously applied magnetic tilt (a); and from a magnetic tilt with simultaneously applied electric asymmetry (b).

compared to a magnetic asymmetry.<sup>20</sup> The magnetic tilt shifts each  $(L_p/2)$  half of the column off the  $r=0$  axis (in opposite directions) by a  $z$ -averaged amount

$$\bar{\Delta}_B = \frac{1}{2} \alpha_B (L_p/2). \quad (6)$$

Simple electrostatics suggests that electric asymmetry voltages  $\pm V_a$  applied to wall sectors of length  $L_a$  will shift each half of the column off-axis by a  $z$ -averaged amount

$$\Delta_E \approx 0.51 R_w \left( \frac{V_a}{2eN_L} \right) \left( \frac{L_a}{L_p/2} \right) \equiv \frac{1}{2} \alpha_E (L_p/2). \quad (7)$$

Here, the numerical coefficient represents the  $m_\theta = 1$  Fourier component of the applied voltage.<sup>20</sup> These center-of-mass shifts can be directly measured by rapidly “cutting” the plasma axially, then dumping and measuring only the section of interest.

With this definition of electric tilt angle  $\alpha_E$ , the electric “tilt” transport of Fig. 11(a) looks identical to the magnetic tilt transport of Eq. (5). The experiments thus determine a rather complete scaling for electric and magnetic tilt-induced transport, as

$$\frac{\nu_p}{\gamma_a} \approx (6.3 \times 10^{-5}) \left( \frac{N_L^u}{N_L} \right) \left( \frac{eN_L^2}{B} \right) \left( \frac{L_p}{R_w} \right)^2 [\alpha_B + \alpha_E]^2, \quad (8)$$

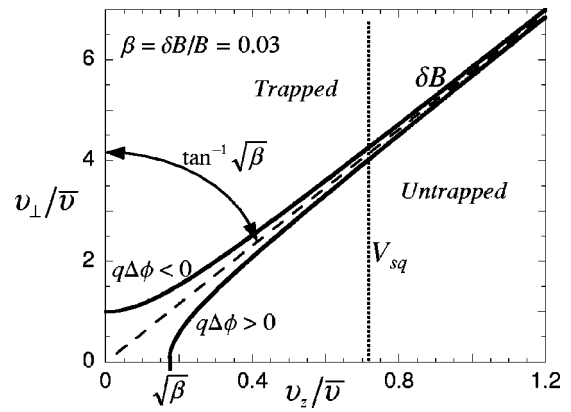


FIG. 12. Velocity-space separatrices for magnetostatic and/or electrostatic trapping.

where  $\alpha = \alpha_x \hat{x} + \alpha_y \hat{y}$ , and Eq. (1) was used for  $N_L^{\text{tr}}$ . We note that the  $\alpha_B \cdot \alpha_E$  cross term is only approximate, since the electric asymmetry is applied only at discrete  $z$  positions, so  $\Delta_E(z) \neq z \alpha_E$ .

## V. TRANSPORT FROM MAGNETIC TRAPPING

Axial variations  $\delta B(z)$  in the magnetic field also cause trapped particles, with the dissipation from separatrix crossings having similar consequences for asymmetry-induced transport. Moreover, our experiments suggest that exceedingly small magnetically trapped populations cause significant asymmetry-induced transport. The magnetic trapping effects have been studied using an axially centered coil which generates a magnetic mirror of strength  $\beta \equiv (\delta B/B) \leq 4\%$  at  $B = 1 \text{ kG}$ ; and also using the ripples of strength  $\beta \approx 10^{-3}$  inherent in our superconducting solenoid.

One expects particles with small pitch angle to be trapped, giving a simple magnetic separatrix defined by  $v_z/v_\perp = \beta^{1/2}$ , shown by the long dashes in Fig. 12. The fraction of these trapped particles is expected to scale as  $\beta^{1/2}$ , giving  $0.03 \leq N_L^{\text{(tr)}}/N_L \leq 0.2$  for our experiments.

The trapped particles can be directly detected by selective dumping techniques, but the relevant parallel velocities are substantially less than  $\bar{v}$ , so measurements to date are only qualitative. Moreover, there are theoretical and experimental reasons to expect that the mirror field causes the electrostatic potential in the plasma to vary along a field line,<sup>27</sup> giving separatrices as shown by the solid curves in Fig. 12. More significantly, an applied electric squeeze voltage  $V_{sq}$  can move the separatrix, allowing direct control of magnetic trapping effects, as will be shown below.

The magnetically trapped particles presumably enable some sort of mode analogous to that observed with electric trapping; but this magnetic mode remains ill-defined. Experiments to date suggest that the mode is either very strongly damped ( $\gamma_a^{(M)}/f_a^{(M)} \geq 0.1$ ), or zero frequency ( $f_a^{(M)} = 0$ ). Moreover, the lack of radial separation between trapped and untrapped particles makes  $f_a^{(M)} = 0$  plausible, since the charge separation and  $\mathbf{E} \times \mathbf{B}$  drifts characterizing the electric mode may not occur.

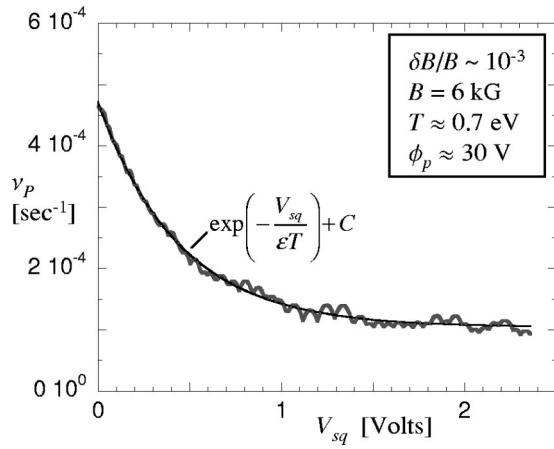


FIG. 13. Reduction of the transport rate  $\nu_p$  with applied  $V_{sq}$ , as particles are excluded from the original magnetic separatrix.

Fortunately, the transport effects of magnetic trapping are more readily observed than the mode itself. Experiments with controlled  $\delta B/B$  and magnetic or electric tilt asymmetries show that the transport from magnetic trapping is quite similar to that from electric trapping. Essentially, the transport follows from the dissipative separatrix crossings, independent of any details of the mode; measuring  $\gamma_a$  merely quantifies this dissipation.

Even though we cannot measure  $\gamma_a^{(M)}$  directly, the experiments suggest that transport from magnetic trapping has essentially the same scalings as in Eq. (8) for electric trapping, with one surprising exception: the transport from magnetic trapping appears to be *independent* of trapping fraction  $N_L^w/N_L \sim (\delta B/B)^{1/2}$  over a wide range. That is, preliminary experiments suggest that

$$\nu_p^{(M)} \propto (N_L^w/N_L)^0 (eN_L^2/B)^1 (L_p/R_w)^2 [\alpha_B + \alpha_E]^2. \quad (9)$$

Even small  $\delta B/B$  can have significant transport effects.

The transport from magnetic trapping can be decreased, however, by altering the separatrix at low  $v_{||}$ . Figure 13 shows that a small electric squeeze applied to the magnetic mirror region decreases  $\nu_p$  by up to 5 times. Moreover, the exponential dependence on  $V_{sq}$  is consistent with a Maxwellian distribution of particles being excluded from trapped-untrapped crossings, as pictured in Fig. 12. At larger values of  $V_{sq}$ , the diffusion across the electric separatrix becomes dominant, and  $\nu_p$  increases with  $V_{sq}$  (not shown).

Separate experiments in which the plasma confinement region did not include the magnetic ripple peak show essentially the same reduction in  $\nu_p$ . The original magnet position in the CamV apparatus results in a magnetic perturbation peak inside the containment region. After moving the magnet by  $\Delta z = 9$  cm, we are able to confine the plasma in a ripple-free region between adjacent magnetic peaks. This results in the same factor of 5 decrease in the background transport rate as does applying a small electric squeeze. In addition, for the ripple-free plasma  $\nu_p(V_{sq})$  has a minimum at  $V_{sq} = 0$  since there is no magnetic separatrix to destroy.

Alternately, the transport effects from magnetic separatrix crossings can be *enhanced* by applying an rf field which scatters particles with resonant parallel velocities.<sup>17</sup> Figure

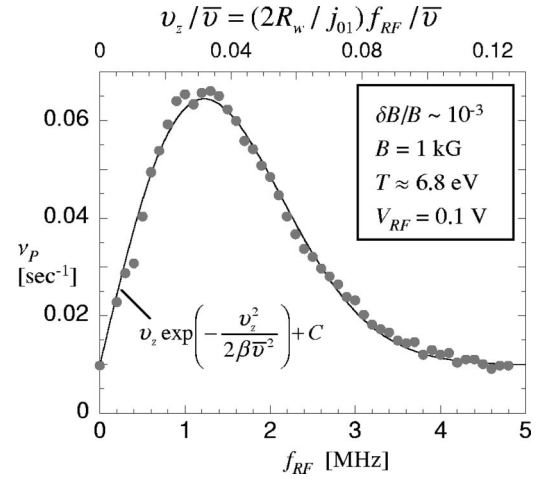


FIG. 14. An applied rf field at frequency  $f_{rf}$  causes enhanced separatrix crossings for resonant electrons, increasing  $\nu_p$ .

14 shows the transport enhancement when a rf wiggle ( $0.1V_{p-p}$ ) at 0.2–5 MHz is applied near a magnetic minimum. Here, we have utilized the “sheath transport” resonance to interact with particles with small  $v_z$ : electrons receive a nonadiabatic kick if they have  $v_z \approx L^* f_{rf}$ , where  $L^* \equiv 2R_w/j_{01}$  is the axial extent of the electric fields from the applied rf drive. The transport response peak in Fig. 14 is as expected for a Maxwellian distribution of particles along the naive ( $\Delta\phi=0$ ) magnetic separatrix of Fig. 12. The more subtle effects of (radially dependent) potential variations,<sup>27</sup> if significant, have yet to be determined.

These trapping experiments strongly suggest that the ill-understood “background” transport and loss observed in many long cylindrical traps is dominated by magnetic trapping and magnetic asymmetries. As caveat, we note that the scalings of Eqs. (8) and (9) are only valid for a single central trapping region, whereas noncentral (or multiple) barriers might exist in a long trap. Also, Eq. (9) for magnetic trapping is still incomplete, since  $\gamma_a^{(M)}$  is unknown.

Nevertheless, the scalings of Eq. (8) show striking correspondence to many prior results on asymmetry-induced transport. For magnetic field, we expect  $\nu_p \propto \gamma_a(B) B^{-1} \propto (B^{-1.5} \text{ to } B^{-2})$ , using the  $\gamma_a(B)$  scaling of electric trapping. The observed length dependence of  $\nu_p$  varies from  $\nu_p \propto L_p^2$  for fixed magnetic tilt  $\alpha_B$  (open and solid circles in Fig. 7), to  $\nu_p \propto L_p^{-2}$  for electric asymmetries, since fixed  $V_a$  and  $L_a$  give  $\alpha_E \propto L_p^{-2}$  in Eq. (7). The oft-observed (and oft-violated)  $L^2/B^2$  scaling<sup>4</sup> for “anomalous” background transport probably results from magnetic asymmetries acting on magnetically trapped populations in low rigidity plasmas. However, the scalings of Eq. (8) will not directly apply to plasmas with noncentered or multiple trapping barriers, so the observation of other length scalings<sup>5,7</sup> is not surprising.

The temperature dependence of  $\nu_p$  is due only to the mode damping rate  $\gamma_a(T)$ , which decreases exponentially in the regions of prior experiments. This probably explains the abrupt decrease<sup>7</sup> in transport observed for rigidity  $\mathcal{R} \gtrsim 10$ . More importantly,  $\mathcal{R}$  is not a globally relevant scaling parameter for transport due to trapped particle separatrix crossings, since unperturbed particle parameters such as  $f_b$  and  $f_E$

cannot describe the nonlinearities of trapped orbits and non-Maxwellian separatrix velocity distributions.

The trapped particle modes and asymmetry-induced transport have been discussed here from the perspective of azimuthal variation  $m_\theta=1$  and axial variation  $k_z=1$ . Trapped particle modes and damping have been observed for  $m_\theta=1, 2$ , and  $3$ ; and multiple trapping barriers would correspond to  $k_z=2, 3, \dots$ . Presumably, a static asymmetry with given  $m_\theta, k_z$  will produce bulk transport by coupling to the separatrix crossings with the same geometry.

## VI. CONCLUSION

A new mechanism of asymmetry-induced bulk radial transport has been developed for non-neutral plasmas with locally trapped particles. The transport arises from the dissipative scattering of particles across the velocity-space separatrix between trapped and passing particles. Since the separatrix crossings also damp the trapped-particle mode, the transport rate is proportional to the damping rate of the mode. For electric trapping, this proportionality has been quantitatively established by experiments. The complicated dependencies of the transport rate on temperature and density profiles can then be determined from the easily measured trapped-particle mode damping rate. The normalized transport rate  $\nu_p/\gamma_a$  has simple scalings for all other plasma parameters. Both experiments and theory quantitatively characterize the mode behavior, and show that the mode damping is due to the separatrix crossings.

Magnetic trapping effects studied here lead us to believe that the asymmetry-induced transport observed in many axially long traps is dominated by this separatrix dissipation, even when no trapping potentials are intentionally applied. Even small magnetic field ripples apparently produce an important loss channel similar to those in toroidal magnetic confinement systems. However, the modes and separatrix dissipation arising from magnetic trapping are not yet understood quantitatively.

In general, velocity-space diffusion across a trapping separatrix is not the only possible mechanism linking azimuthal asymmetries to bulk radial transport. Comparing trapped-particle transport to other transport mechanisms in a

variety of apparatuses may contribute substantially to our understanding of plasma transport processes.

## ACKNOWLEDGMENTS

The authors gratefully acknowledge extensive theory discussions with T. J. Hillsabeck and T. M. O'Neil.

This work was supported by National Science Foundation Grant No. PHY-9876999 and Office of Naval Research Grant No. N00014-96-1-0239.

- <sup>1</sup>*Non-Neutral Plasma Physics IV*, edited by F. Anderegg, AIP Conf. Proc. **606** (American Institute of Physics, Melville, NY, 2002).
- <sup>2</sup>T.M. O'Neil, Phys. Fluids **23**, 2216 (1980).
- <sup>3</sup>J.H. Malmberg and C.F. Driscoll, Phys. Rev. Lett. **44**, 654 (1980).
- <sup>4</sup>C.F. Driscoll, K.S. Fine, and J.H. Malmberg, Phys. Fluids **29**, 2015 (1986).
- <sup>5</sup>J. Notte and J. Fajans, Phys. Plasmas **1**, 1123 (1994).
- <sup>6</sup>B.P. Cluggish, Ph.D. thesis, University of California, San Diego, 1995.
- <sup>7</sup>J.M. Kriesel and C.F. Driscoll, Phys. Rev. Lett. **85**, 2510 (2000).
- <sup>8</sup>E.H. Chao, R.C. Davidson, S.F. Paul, and K.A. Morrison, Phys. Plasmas **7**, 831 (2000).
- <sup>9</sup>D.L. Eggleston and B. Carrillo, in *Non-Neutral Plasma Physics IV*, edited by F. Anderegg, AIP Conf. Proc. **606** (American Institute of Physics, Melville, NY, 2002), pp. 369–377.
- <sup>10</sup>D.L. Eggleston and T.M. O'Neil, Phys. Plasmas **6**, 2699 (1999).
- <sup>11</sup>B.B. Kadomtsev and O.P. Pogutse, Sov. Phys. JETP **24**, 1172 (1967).
- <sup>12</sup>W.M. Tang, Nucl. Fusion **18**, 1089 (1978).
- <sup>13</sup>M.N. Rosenbluth, D.W. Ross, and D.P. Kostomarov, Nucl. Fusion **12**, 3 (1972).
- <sup>14</sup>G.A. Navratil, A.K. Sen, and J. Slough, Phys. Fluids **26**, 1044 (1983).
- <sup>15</sup>A.A. Kabantsev, C.F. Driscoll, T.J. Hillsabeck, T.M. O'Neil, and J.H. Yu, Phys. Rev. Lett. **87**, 225002 (2001).
- <sup>16</sup>T.J. Hillsabeck, A.A. Kabantsev, C.F. Driscoll, and T.M. O'Neil, "Damping of the trapped-particle diocotron mode," Phys. Rev. Lett. (submitted).
- <sup>17</sup>A.A. Kabantsev and C.F. Driscoll, Rev. Sci. Instrum. **74**, 1925 (2003).
- <sup>18</sup>G.W. Hart, Phys. Fluids B **3**, 2987 (1991).
- <sup>19</sup>K.S. Fine, W.G. Flynn, A.C. Cass, and C.F. Driscoll, Phys. Rev. Lett. **75**, 3277 (1995).
- <sup>20</sup>J.M. Kriesel, Ph.D. thesis, University of California, San Diego, 1999.
- <sup>21</sup>G.W. Mason, Phys. Plasmas **10**, 1231 (2003).
- <sup>22</sup>X.-P. Huang, F. Anderegg, E.M. Hollmann, T.M. O'Neil, and C.F. Driscoll, Phys. Rev. Lett. **78**, 875 (1997).
- <sup>23</sup>F. Anderegg, E.M. Hollmann, and C.F. Driscoll, Phys. Rev. Lett. **81**, 4875 (1998).
- <sup>24</sup>B.R. Beck, J. Fajans, and J.H. Malmberg, Phys. Rev. Lett. **68**, 317 (1992).
- <sup>25</sup>B.P. Cluggish, J.R. Danielson, and C.F. Driscoll, Phys. Rev. Lett. **81**, 353 (1998).
- <sup>26</sup>E. Sarid, E. Gilson, and J. Fajans, Phys. Rev. Lett. **89**, 105002 (2002).
- <sup>27</sup>J. Fajans, Phys. Plasmas **10**, 1209 (2003).